Journal of Microscopy, Vol. 180, Pt 3, December 1995, pp. 263–276.
Received 24 April 1995; accepted 17 August 1995

Energy-filtered Fresnel contrast analysis of Fe/Cu multilayers

R. E. DUNIN-BORKOWSKI, C. B. BOOTHROYD, S. J. LLOYD & W. M. STOBBS
Department of Materials Science and Metallurgy, Pembroke Street, Cambridge CB2 3QZ, U.K.

Key words. Energy filtering, Fresnel contrast, Fe/Cu multilayers.

Summary

Energy-filtered imaging in the transmission electron microscope is applied to the Fresnel contrast exhibited by a fine-period Fe/Cu multilayer. Comparisons of filtered and unfiltered image series demonstrate the effects of inelastic scattering, and it is shown that the use of energy filtering allows improved confidence in the physical origins of the contrast for a specimen, such as that described, for which the structure is still uncertain.

1. Introduction

Fresnel contrast analysis in the transmission electron microscope (TEM) can be used to determine the compositional abruptness of interfaces in layered systems (Stobbs & Ross, 1989). The method relies on the sensitivity of the elastic rather than the inelastic scattering of electrons to local changes in the projected potential, and the numerical approaches that can be used in such analyses are described by Ross & Stobbs (1991a) for different types of problem. However, the fact that electrons are also inelastically scattered within the specimen affects both the magnitude and the details of the Fresnel contrast at an interface. This is particularly important at the low defocus values that are potentially most sensitive to the form of a near atomically abrupt interface.

For example, in an assessment of the abruptness of the Si/SiO_2 interface using the Fresnel method (Ross & Stobbs, 1991b), the accuracy to which the data could be interpreted was limited by uncertainties in the contrast changes caused by inelastically scattered electrons. Centre-stop lattice imaging, as applied by Boothroyd & Stobbs (1988, 1989) to the analysis of the form of AlGaAs multilayers, is also strongly affected by inelastic scattering within both the specimen and the amorphous layers on its surface. The effects of inelastic scattering are potentially of greater importance in the analysis of high-resolution electron microscopy (HREM) contrast (Stobbs & Saxton, 1988) than in Fresnel imaging, and the effects of not considering such contributions in the analysis of high-resolution images have recently been assessed quantitatively (Boothroyd *et al.*, 1994). That Fresnel contrast analysis is not normally as strongly affected by inelastic scattering has its origins in the fact that the defoci used are generally disproportionately larger than in high-resolution analysis.

However, this need not be the case, and in principle the form of a near-to-atomically abrupt interface is best analysed by the Fresnel approach using defoci which are not significantly greater than are those used for high-resolution images. Accordingly, if the Fresnel method is to be applied to such problems then either the effects of inelastic scattering need to be included in the modelling of the data or energy-filtered imaging should be used. Unfortunately, the effects of inelastic scattering are difficult to model theoretically, both because of their complexity and because the coherence of the scattering process (i.e. the degree to which phase information is retained) is not readily predictable as a function of scattering angle (Howie, 1963), and would thus be expected to vary across a localized rigid body displacement at an interface.

It is for these reasons that, just as in HREM, most Fresnel analyses to date have concentrated on the assessment of pattern changes with defocus, absolute intensities rarely being compared with simulations. Until quantitative matches of absolute values of the observed and simulated Fresnel contrast have been obtained for known interfaces, doubts should be retained about the validity of the application of the Fresnel method, even if this has still not been achieved unambiguously for the high-resolution approach. The use of energy-filtered imaging should facilitate the quantitative comparison of experimental and theoretical data by removing the inelastic scattering contribution from the contrast. In the future, the comparison of such filtered data with low-loss Fresnel contrast should also allow the coherence and the localization of inelastic scattering processes to be better understood.

Here, we present the first direct investigation of the effect of inelastic scattering on Fresnel contrast, using energy-filtered imaging to characterize the Fresnel contrast

exhibited by a fine-period coherent Fe/Cu multilayer. The magnitude of the experimental contrast is related to simulations which incorporate data on compositional and structural variations within the specimen as obtained, particularly in the latter context, with only limited confidence by other means. Conclusions can nonetheless be drawn about the degree to which energy-filtered imaging is required for the true quantitative analysis of such experimental data. Furthermore, while the abruptness of the interfaces in this specimen has not been assessed independently, it is demonstrated that the use of energy filtering in Fresnel imaging allows a considerable improvement in the confidence to which inferences can be drawn on the lattice spacing variations in the multilayer.

Interest in the characterization of fine-period Fe/Cu multilayers, which can be grown on (001) Cu, has its origin in the fact that thin Fe layers can be retained with a nonequilibrium coherently strained face centred structure, whose magnetic state is very sensitive to the structural and chemical abruptness of the interfaces between the layers (Moruzzi *et al.*, 1989). Recent results on Fe lattice spacings have shown substantial differences from the values that would be predicted using conventional elasticity theory (Lloyd *et al.*, 1995), and now need to be correlated with physical property data. However, the quantitative modelling of the lattice strains requires a knowledge of the interface abruptness, and this can be assessed using the Fresnel approach. Furthermore, as we will see below, and given the use of filtering to improve the reliability of the Fresnel data, the analysis of the Fresnel contrast provides important confirmatory evidence for the anomalous nature of the lattice strains in the Fe.

We describe the qualitative effects of energy filtering on the Fresnel contrast in section 3 and discuss the quantitative assessment of the structure of the multilayer using the Fresnel approach in Section 4.

2. Experimental details

The specimen examined here was a 2·35-nm-wavelength coherently strained $(Fe_4/Cu_9)_{100}$ multilayer of face centred structure, grown on (001) Cu by UHV DC magnetron getter sputtering (Somekh & Baxter, 1986). The notation used to describe the multilayer indicates that it contains 100 periods of a unit which nominally consists of four atomic layers of Fe and nine atomic layers of Cu. Energy-dispersive X-ray spectroscopy (EDXS) analysis of the average composition within the multilayered region indicated an Fe/Cu ratio within half a monolayer of that specified (Lloyd *et al.*, 1995). The specimen was prepared for TEM examination of the layering in an edge-on orientation by floating the multilayer off its rock salt substrate, copper plating, mechanically grinding to a wedge and ion beam thinning with Ar at 5 kV.

Energy-filtered images of the multilayer were obtained using a JEOL 4000FX microscope ($C_S = 2{\cdot}0$ mm, $C_C = 1{\cdot}4$ mm), equipped with a post-column Gatan imaging filter (GIF) and operated at 400 kV. The modified objective lens in this microscope, which has a further minilens fitted into its lower bore, allows reduced magnifications to be obtained prior to the spectrometer. Under these conditions, the normal selected-area aperture is used as an objective aperture, the minilens being used to make this plane conjugate to the back focal plane of the objective lens. For each series of images, care was taken to ensure that the multilayer was vertical with respect to the incident electron beam, with the specimen tilted a few degrees from [100] about the (001) layer plane normal. It was ensured that diffraction contrast from the crystal was low at the symmetrically excited 001 systematic row at which the layering was accurately edge-on. A 10-eV energy window was used for filtered imaging, and the defocus step size used between successive images in a given image series was 179 nm.

3. The qualitative differences between filtered and unfiltered Fresnel data

Before attempting to analyse the structure of the multilayer in Section 4, we first discuss the major differences in the forms of the filtered and unfiltered Fresnel data for a typical fine-layered structure such as that examined here. It is a feature of the normal use of the Fresnel method for the quantitative assessment of the form of a composition change across an interface that a small objective aperture is used, limiting contrast-reducing contributions from higher angle inelastic scattering. The individual images in a through-focal series are obtained at resolutions which are often a factor of two or three below that to which the form of an interface can be inferred from the series as a whole (e.g. Stobbs & Ross, 1989). However, given that our initial interest here lies in the effects of the inelastic scattering on the contrast, we have chosen to compare filtered and unfiltered image series obtained with no objective aperture,

Fig. 1. Examples of unfiltered and filtered images taken from a through-focal series of a coherent Fe_4/Cu_9 multilayer, for the nominal defocus values indicated. The images were taken on a JEOL 4000FX microscope equipped with a Gatan imaging filter, without using an objective aperture. (The regions shown are 400 × 315 pixels in size.)

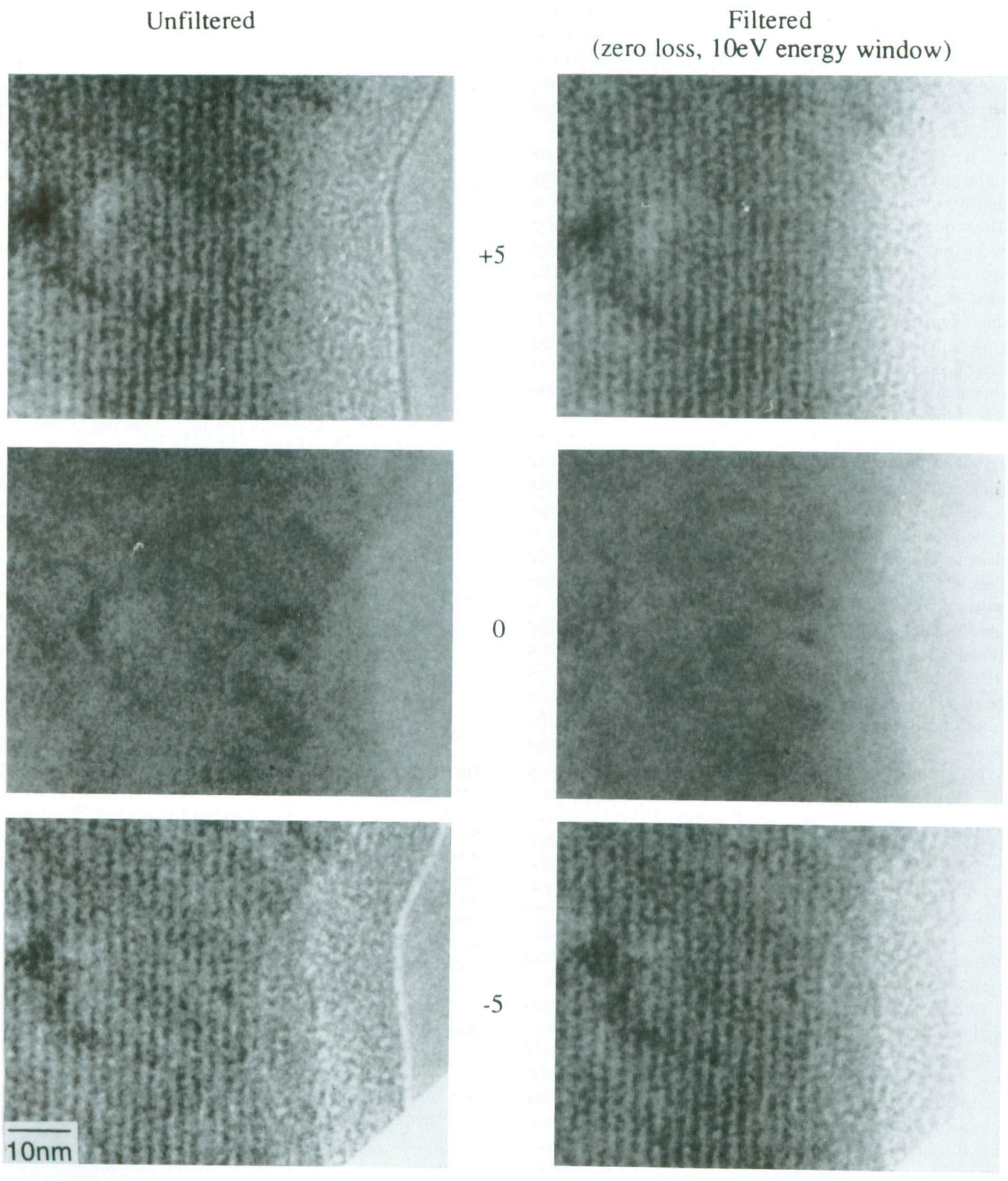
Unfiltered
Filtered
(zero loss, 10eV energy window)
+5
0
-5
10nm
Nominal defocus
(steps of 179nm)

the microscope being used conventionally with the objective minilens switched off. Of course, in principle, if the filtering process satisfactorily restores the full contrast to be expected for the elastic contributions to the image then the larger the objective aperture used the better the data that should be obtained.

The 11 digitally acquired images in each through-focal series were 512×512 pixels in size, with a sampling density of 0·18 nm/pixel and an acquisition time of 2·6 s. The semiconvergence angle of the incident illumination was measured as 0·11 mrad from the width of an unsaturated spot in a diffraction pattern taken at the imaging conditions used for the series. Examples of 400×315-pixel regions, digitally extracted from the raw data, are shown in Fig. 1. Qualitatively, the narrower Fe layers can be seen to exhibit bright contrast overfocus and dark contrast underfocus, and this indicates that the Fe layers have a higher forward scattering potential than the Cu layers.

For a first appraisal of the effects of inelastic scattering on Fresnel contrast, rectangular regions of each image were projected digitally parallel to the direction of the layers over a distance of 60 nm. Examples of the resulting one-dimensional intensity profiles are shown in Fig. 2(a) for a defocus of five steps (measured as 883 nm) overfocus. The Fresnel fringes from each interface can be seen to overlap as a result of the fine periodicity of the layering. It is immediately disturbing to note that the vacuum intensities (outside the specimen) for the unfiltered images are some 10–20% higher than are those for the filtered images. This point will be discussed later, but for the present the vacuum intensities were scaled to unity as shown in Fig. 2(b). The standard procedure of dividing these profiles by smoothed versions of the zero defocus profile in order to take account of 'absorption' (loss of electrons from the image by any process) (see, for example, Ross & Stobbs, 1991c) gives the traces shown in Fig. 2(c). The validity of this approach requires that absorption affects all electrons equally, whether or not they contribute to Fresnel contrast. Reassuringly, although the absolute intensity of the filtered profile in Fig. 2(a) is lower than that of the unfiltered profile, the corresponding fringe contrast in Fig. 2(c) is higher than that of the unfiltered profile.

While the differences in the vacuum levels for the two series are alone sufficient to negate a fully quantitative approach to the analysis of the contrast, some measure of the differences between the individual series and computer simulations is useful, if only to assess the magnitude of any problems associated with not using an objective aperture, as for the images described in this section. This requires a knowledge of the foil thickness. Although foil bending precluded the use of an accurate weak-beam approach, the local specimen thickness could be obtained from the ratio of the unfiltered intensity (I_{tot}) to the filtered intensity (I_{el}) in multiples of the total inelastic mean free path (λ_{in}) by using

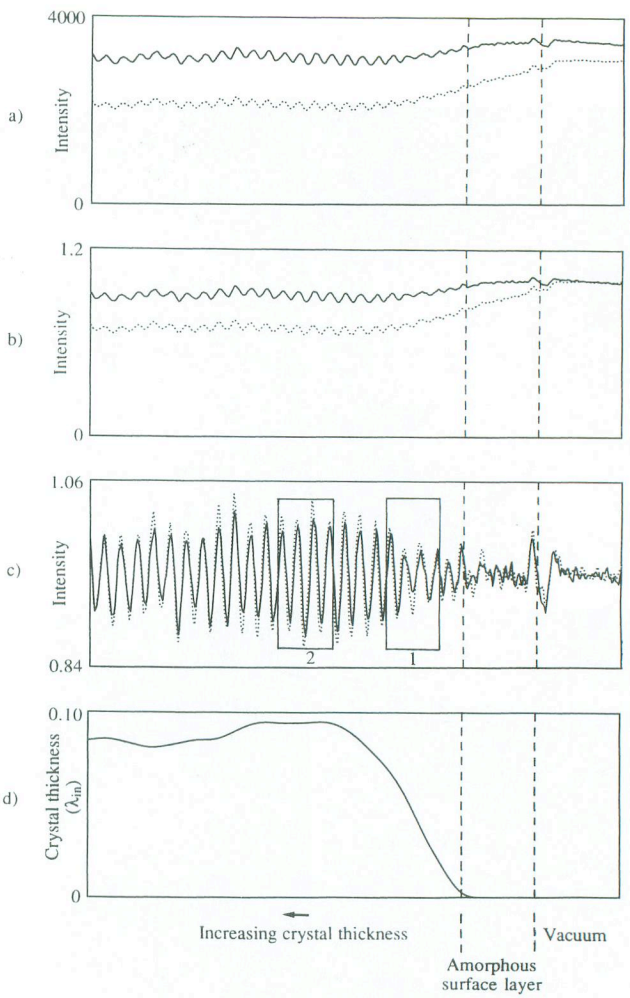

Fig. 2. Analysis of the images taken at a defocus of five steps (measured as 883 nm) overfocus, for both unfiltered (——) and filtered (. . . . .) data: (a) projections of the raw unfiltered and filtered data parallel to the layers over a distance of 60 nm (330 pixels); (b) now with the vacuum intensities (i.e. outside the specimen) scaled to unity; and (c) divided by a smooth background. (d) The crystal thickness profile in multiples of the total inelastic mean free path λ_{in}, determined from the images shown in (b) using the method outlined in the text. The regions marked 1 and 2 correspond to mean crystal thicknesses of $0{\cdot}05\lambda_{in}$ and $0{\cdot}09\lambda_{in}$, respectively.

the relation:

$$(t/\lambda_{in}) = \ln(I_{tot}/I_{el})$$

(Egerton, 1986). This approach does not distinguish directly between an amorphous surface layer, resulting from ion beam damage and sputter contamination during ion beam thinning, and the crystalline region giving rise to the Fresnel contrast: a finite value for the specimen thickness is thus obtained at zero *crystal* thickness. To first order, the presence of the surface layer can be taken into account by scaling the intensities of the profiles in Fig. 2(b) to unity at

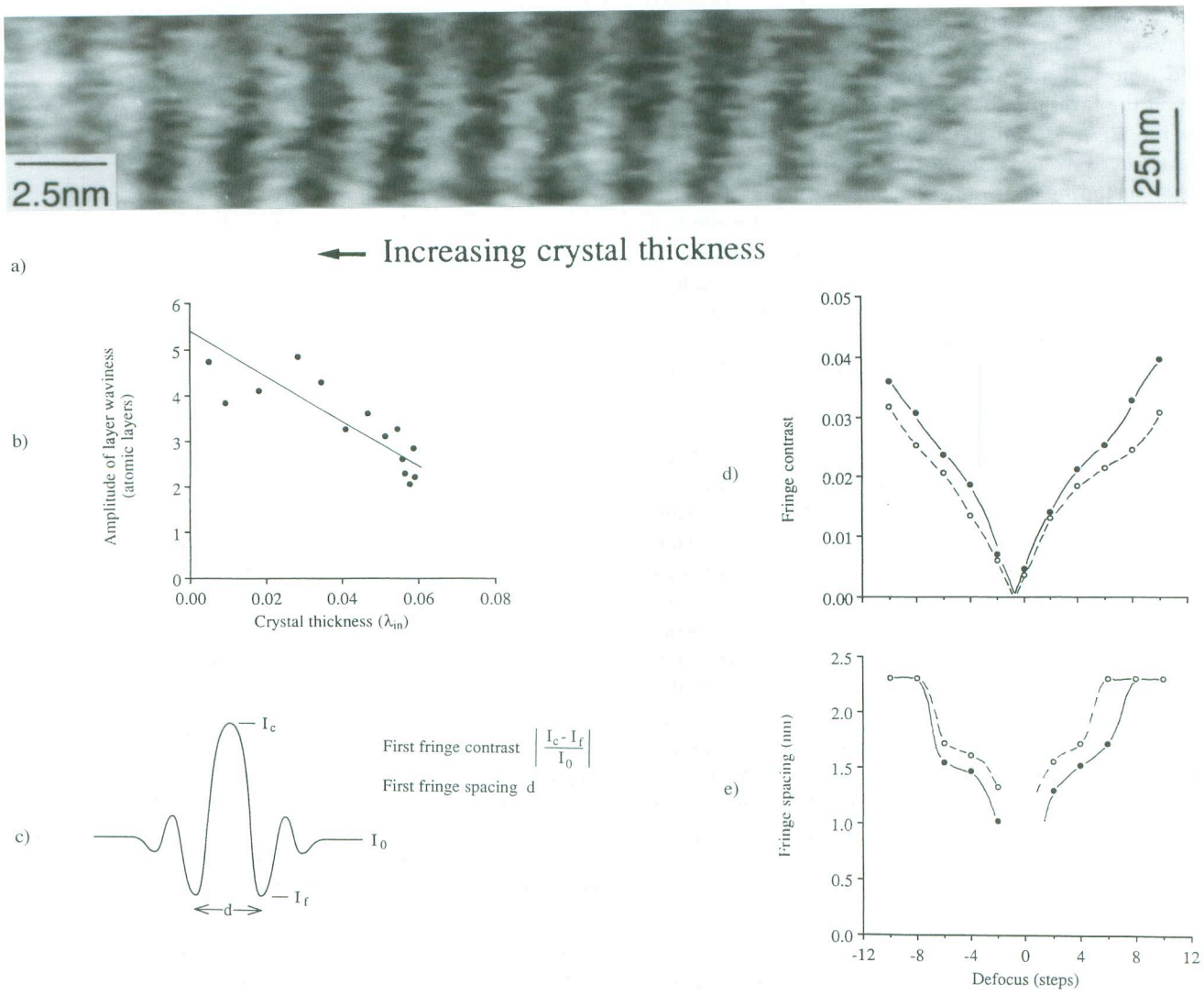

Fig. 3. Illustration of coarse long-range irregularities in the layer spacings: (a) a region of the five-step overfocus image, with the vertical spatial scale compressed; (b) amplitude of layer waviness (peak-to-peak) as a function of crystal thickness for the image shown in (a); (c) definitions of Fresnel fringe contrast and spacing used in this paper; (d, e) fringe contrast and spacing, respectively, plotted both with (——) and without (- - -) distortions removed by artificially straightening the layers, for a specimen thickness of $0{\cdot}05\lambda_{in}$.

zero *crystal* thickness, i.e. at the position of the left-hand vertical dashed line marked in the figure. This treatment relies on the assumption that the sole effect of the amorphous layer is to remove equal proportions of all electrons (i.e. those contributing and not contributing to Fresnel contrast) from the image. The resulting (smoothed) graph of crystal thickness, plotted in multiples of λ_{in}, is shown in Fig. 2(d). The fringes which were chosen for further analysis are marked in Fig. 2(c), at thicknesses which were measured (using the graph in Fig. 2(d)) to have average values of $0{\cdot}05\lambda_{in}$ and $0{\cdot}09\lambda_{in}$. The calculated value of λ_{in} for Cu at 400 kV is 68 nm (Egerton, 1986). It is noteworthy in passing that the experimental data of Munoz (1983) and Cheng (1985), as presented by Egerton (1986) and converted to 400 kV for scattering to all angles, give values for λ_{in} which are as large as 150 nm. However, the form of the general contrast exhibited by the layering is such that we can preclude a thickness for the regions examined as large as this latter figure would imply, and we have accordingly used the theoretical value of 68 nm for λ_{in}.

Wavy layers

As a subsidiary but important point, the original images were found to exhibit coarse long-range (≈25-nm) irregularities in the spacings of the layers. These can be seen more clearly in Fig. 3(a) with the vertical spatial scale of the five-step overfocus image compressed. Not surprisingly, the amplitude of the waviness of each layer (plotted in Fig. 3b) indicates that the layers appear less distorted and exhibit

reduced contrast, at higher specimen thickness because the waviness is then averaged as the beam passes through the foil. In a normal quantitative analysis of the composition profile of the layering, this effect would preclude the direct use of the Fresnel technique for the higher foil thicknesses. However, here we are interested more in the effects of the inelastic scattering as a function of increasing foil thicknesses, so a first-order approach to correct for the effect of the layer waviness was obtained by straightening out the individual fringe systems along their average orientation before obtaining their projecting intensities. In order to illustrate the effect of straightening the layers on the data, graphs of fringe contrast and spacing (as defined in Fig. 3c) are plotted as a function of defocus in Fig. 3(d) and (e), respectively, for the fringes marked in Fig. 2(c) at a measured crystal thickness of $0{\cdot}05\lambda_{in}$, for the profiles both with and without the waviness straightened out. Straightening the fringes results in their measured contrast being greater, and the spacings of the subsidiary fringes in each layer are smaller because each layer is effectively thinner in projection. Other TEM samples from this particular multilayer have previously been assessed using unfiltered Fresnel techniques (Lloyd *et al.*, 1994) in regions exhibiting lower layer waviness, and the spacings of the fringes in the specimen described here match those measured previously only when the long-range distortions are removed. It should be noted that the straightening method described does not of course alter the local layer contrast which is still reduced in a thick foil region relative to that which would have been seen for a locally flat layer.

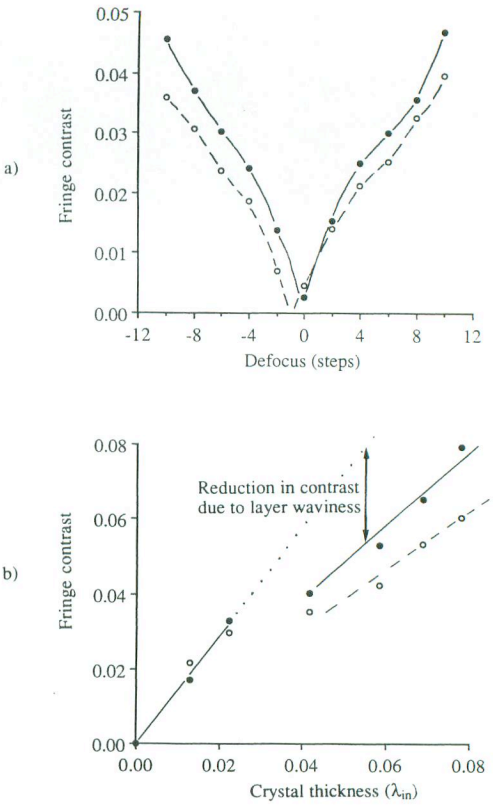

Fig. 4. Fringe contrast plotted as a function of (a) defocus for a specimen thickness of $0{\cdot}05\lambda_{in}$, and (b) specimen thickness for a defocus of 10 steps overfocus (one step = 179 nm). Both the filtered (—) and the unfiltered (- - -) data have had long-range distortions removed by artificially straightening the layers.

The effects of filtering on the form of the contrast

Having dealt to first order with the potentially confusing effects of both the amorphous surface layers and the multilayer waviness, we can now compare the experimental data with simulations in order to investigate the effects of energy-filtered images on the form, if not the magnitude, of the Fresnel contrast. To facilitate analysis of the filtered and unfiltered experimental profiles, the fringes marked in Fig. 2(c) were first averaged and symmetrized to remove the effects of any small local crystal tilt. The dramatic effect of filtering on the measured contrast is clear in Fig. 4(a). We can firstly note that the extrapolated minimum contrast point for the unfiltered data is at a lower objective current than for the filtered data by ≈100 nm. The shift in focus is of the expected order of magnitude in that the calculated shift overfocus of inelastically scattered electrons, for a plasmon energy loss of $\Delta V = 23$ eV, is 140 nm at an accelerating voltage of 400 kV. Examining the form of the contrast change with defocus, we can see that not only is the contrast at this thickness some 10–20% higher after filtering, but it also behaves more symmetrically with focus. In general, it is a signature of the presence of inelastic contributions to the Fresnel contrast when, as here, the unfiltered data exhibit lower contrast underfocus than overfocus (e.g. Ross & Stobbs, 1991a). When the fringe contrast is plotted as a function of crystal thickness, as shown in Fig. 4(b), the unfiltered and filtered signals are similar when the specimen is thin (because there is then only a relatively small inelastic contribution), but diverge as the specimen becomes thicker. It should be remembered that the effects of the waviness of the layers were removed by 'straightening', as described above. Examining the filtered contrast data, we can now see that the effect of this procedure has been to split the data into two regimes: one for small thicknesses and one for thicknesses above which the straightening method does not increase the contrast because of the effects of projection. This is why, although it is possible to draw a single curve through the filtered data in Fig. 4(b), it is more reasonable to draw two straight lines, one for the data obtained at low thicknesses and one for the data at thicknesses at which there is a retained reduction in the Fresnel contrast due to layer waviness. It is clear that the line for the data obtained at high specimen thicknesses extrapolates to zero contrast at

zero thickness as it should, and on this basis the reduction in the contrast due to layer waviness is about 30% at higher specimen thickness. It should be noted that in the unfiltered data the effects of inelastic scattering superposed on the effects of the layer waviness partially disguise the trend due to the latter effect. Nevertheless, it remains clear that the divergence of the filtered and unfiltered data in Fig. 4(b) as a function of thickness is qualitatively as would be expected for a progressively increasing fraction of higher loss electrons reducing the unfiltered contrast. Qualitatively, the graphs in Fig. 4 are thus in agreement with the predicted effects both of the layer waviness and of the inelastic scattering.

We now need to make a preliminary assessment of the degree to which the magnitude of the filtered and unfiltered contrast data agree with theoretical predictions. The averaged experimental contrast data are shown in Fig. 5(a) for a crystal thickness of $0{\cdot}09\lambda_{in}$. One-dimensional mean potential simulations,* as described by Ross & Stobbs (1991a) and following the approach of Ness *et al.* (1986), are shown in Fig. 5(b) both for the filtered and for the unfiltered images at a specimen thickness of 6·1 nm (i.e. $0{\cdot}09\lambda_{in}$ with $\lambda_{in} = 68$ nm). The simulations were obtained using the mean potential profile shown in Fig. 5(c), for which it was assumed that the local roughness of the layering (as distinct from its longer range waviness) causes 'intermixing' in the projected potential over two atomic layers. This model provided the best qualitative fit for data previously obtained for similar but less wavy layers of the same specimen (Lloyd *et al.*, 1994). The sampling density used for the simulations was 0·00229 nm/pixel and all other parameters were as for the experimental images. For the unfiltered simulations at this specimen thickness of $0{\cdot}09\lambda_{in}$, 9% of the incident electrons were taken to be overfocused with respect to the elastically scattered electrons by an amount corresponding to the energy of a plasmon loss. As a first-order approximation for the contribution that the loss electrons would make to the contrast (Stobbs & Saxton, 1988), it was assumed that their contribution is incoherent and that the average specimen thickness giving rise to the contrast is the same as that for the elastically scattered electrons. A value of half the specimen thickness might have been more properly used in this approximation; however, the amorphous layers will increase the proportion of the crystalline material giving rise to elastic scattering of loss electrons. The values of the mean forward scattering potential V_0 to use in the simulations of the strained Fe and Cu were obtained using the scattering factors of Rez *et al.* (1994), and values for lattice spacings were evaluated using conventional elasticity theory on the basis of the multilayer, as viewed in a thin foil, having a minimum strain energy (see Table 1).

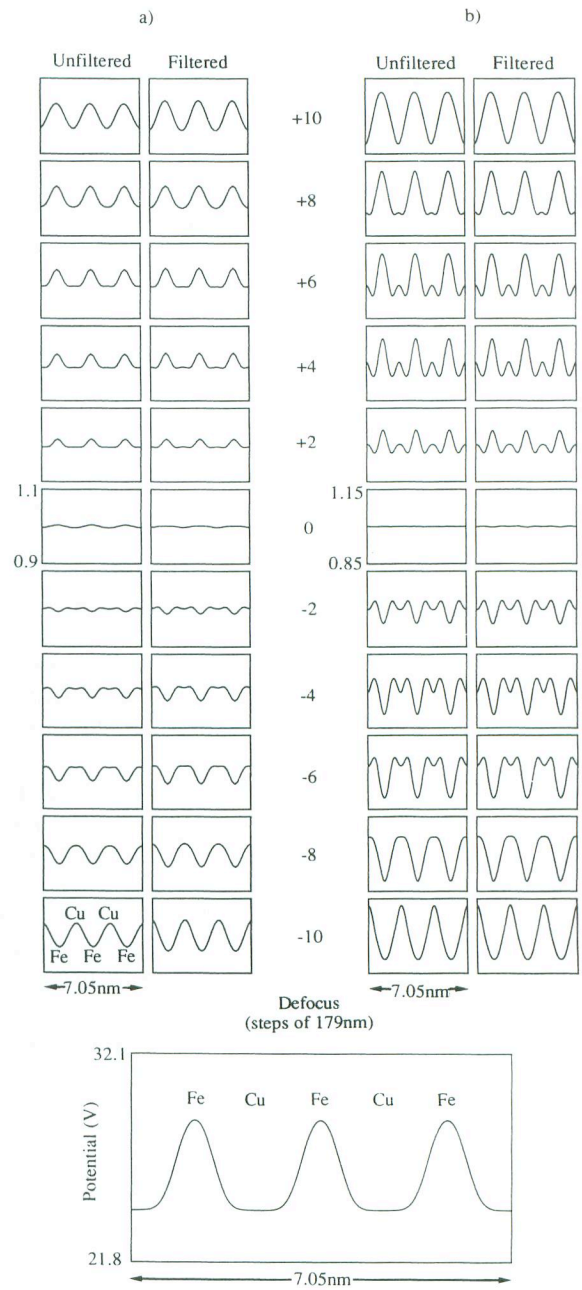

Fig. 5. Comparison of (a) experimental and (b) simulated fringe profiles, for a specimen thickness of $0{\cdot}09\lambda_{in}$ with λ_{in} taken to be 68 nm. (c) The mean forward scattering potential profile used in the simulations, which are described in detail in the text. (The experimental profiles have been averaged over four adjacent fringes and symmetrized.)

*Full atomistic simulations are required for a complete analysis of the data and will affect the fine details in the simulations. However, it is primarily the magnitude of the contrast which is compared here and this is more sensitive to the mean potential. The presence of distortions in the local atomic positions, appropriate for a tetragonally strained f.c.c. Fe layer as suggested by Müller *et al.* (1995), also suggests that the continuum calculation should be more accurate than an atomistic calculation which does not include this reconstruction (or which models it incorrectly).

Table 1. Parameters used for calculating the value of ΔV to use in simulations of the Fe_4/Cu_9 multilayer. The scattering factors used are taken from the data of Rez *et al.* (1994).

	Cu	Fe
Electron scattering factor (nm)	0·6285	0·7140
Stress-free f.c.c. lattice parameter (nm)	0·3615	0·3585
Strained according to conventional elasticity theory		
In-plane lattice parameter (nm)	0·3604	
Out-of-plane lattice parameter (nm)	0·3631	0·3563
V_0 (V)	25·5	29·6
ΔV (V)	4·1	
Strained according to the data of Müller *et al.* (1995)		
In-plane lattice parameter (nm)	0·3604	
Average out-of-plane lattice parameter (nm)	0·3631	0·3740
V_0 (V)	25·5	28·3
ΔV (V)	2·8	

Examining Fig. 5(a), we can again note the reduction in the asymmetry of the contrast with focus after energy filtering. However, comparing both the filtered and the unfiltered experimental results with the simulations in Fig. 5(b), it is also clear that although the same qualitative behaviour is apparent in the simulations (confirming our understanding that it is caused by the addition of inelastically scattered electrons which are overfocused relative to elastically scattered electrons), the simulated filtered contrast is far too high and the effects predicted due to inelastic scattering are far smaller than are those seen experimentally. That the fringe contrast in the experimental unfiltered profiles exhibits much greater asymmetry with defocus than do the simulations indicates either that there is experimentally more inelastic scattering than predicted theoretically or that the contribution to the contrast made by these electrons is far larger than on the basis of the above assumptions. This would be the case if the inelastic contributions were to a degree coherent, which would be the limiting assumption (as discussed by Boothroyd & Stobbs, 1988, 1989) on the basis that the plasmon scattering involves only intraband transitions and is primarily to very low angles with a constant phase change for the loss process (Howie, 1963). However, given that the mean potential simulations for the filtered profiles have a contrast range some 3·3 times higher than that of the experimental profiles, as shown in Table 2, it would be inappropriate to consider the relevance of the inelastic scattering contribution until this more major discrepancy is understood. The discrepancy is far larger than the 30% which might have been expected due to the long-range waviness of the layering. In relation to the physical nature and the form of the multilayer, the most interesting potential origin for the difference would lie in the calculated value for ΔV, as used in the above simulations, being incorrect and far too large. Before assessing this possibility,

Table 2. Experimental values of the magnitude of the fringe contrast for a defocus of six steps and a measured specimen thickness of $0{\cdot}09\lambda_{in}$, together with the discrepancy with mean potential simulations calculated using the theoretical value of $\lambda_{in} = 68$ nm given in Table 3. (The simulations have a contrast of 0·172 for a thickness of $0{\cdot}09\lambda_{in}$ with $\lambda_{in} = 68$ nm.)

	1st experiment		2nd experiment	
Imaging conditions	Contrast	Discrepancy with simulation for $\lambda_{in} = 68$ nm and $\Delta V = 4{\cdot}1$ V	Contrast	Discrepancy with simulation for $\lambda_{in} = 68$ nm and $\Delta V = 4{\cdot}1$ V
Unfiltered (no aperture)	0·042	3·9	0·040	4·3
Filtered (no aperture)	0·050	3·3	0·063	2·7
Unfiltered (with aperture)	—	—	0·058	3·0
Filtered (with aperture)	—	—	0·082	2·1
Filtered (with aperture and corrected for detector response)	—	—	0·095	1·8 (1·2 using $\Delta V = 2{\cdot}8$ V)

it is necessary to determine the degree to which other sources of error, such as the effect of the point spread function of the detector, might be contributing. While we are clear that there cannot be substantial errors arising from inaccuracies in the measurement of the thickness (particularly given that the theoretical value for the mean free path is substantially lower than values which have been reported experimentally (see Egerton, 1986), it remains that there could be problems associated with the use of data obtained without an objective aperture. Accordingly, we obtained further experimental filtered and unfiltered through-focal series using an objective aperture and it is these that are examined below in relation to the magnitude of the observed contrast. The effect of not using an objective aperture was also examined for this new data set.

4. The quantification of images taken using an objective aperture

The synergistic effects of collection angle and inelastic scattering on the contrast

The effect of using an objective aperture was investigated by obtaining images of a different region of the same specimen as that examined above (after rethinning it for several minutes) with the objective minilens of the microscope at a condition such that the normal selected-area aperture plane was conjugate with the back focal plane of the objective lens; the selected-area apertures could thus now be used as virtual objective apertures. The conditions used for imaging were as close to those used for the first series as possible, with a sampling density on the CCD array of the detector of 0·069 nm/pixel, exposure times of 1 s and a measured beam convergence semiangle of 0·08 mrad. Unfiltered and filtered through-focal series were taken both with and without using a virtual objective aperture of semiangle 4·5 mrad. Suitable regions of the images were projected over a distance of 17 nm (250 pixels) to give one-dimensional intensity profiles, such as those shown in Fig. 6(a) for a defocus of four steps overfocus. The vacuum intensities again differed between the sets of images (by 15% between the extreme limits of unfiltered images taken with no aperture and filtered images taken with an aperture), and have been scaled to unity in Fig. 6(a). It should be noted that the intensity of the unfiltered images obtained with no objective aperture decreases less in the amorphous layer than for the first series described above, which is related to the fact that the surface layer was thinner for this set of images. It can be seen from Fig. 6(a) that the presence of an objective aperture does indeed have an effect on the background intensity in the image—its effect on the *contrast* will be described below. It was established above that the use of the ratio of the unfiltered to the filtered background intensity for determining the specimen thickness is affected by the presence of amorphous surface layers—this is illustrated dramatically in Fig. 6(b), which shows the specimen thickness calculated using the same relation both with and without scaling the intensity at zero *crystal* thickness to unity. The specimen thicknesses determined with and without taking account of the amorphous layer are clearly grossly different: a point to be generally aware of when measuring specimen thicknesses using electron energy-loss spectroscopy (see also Dobson *et al.*, 1991). Figure 6(c) and (d) show calculations of the fractions of the total intensity in the images scattered elastically and inelastically both into and out of the objective aperture. The graphs are drawn with and without compensating for the presence of the surface layer and are derived from smoothed versions of the profiles shown in Fig. 6(a). Figure 7 shows theoretical versions of the graphs in Fig. 6(c, d), calculated for values of λ_{in} equal to both λ_{el} and $3\lambda_{el}$ (assuming single scattering, and 82 and 30% of the scattered inelastic and elastic intensity retained in the aperture, respectively, as calculated for Cu in Table 3). (The latter value for λ_{in} corresponds to the experimental values in Egerton (1986) which were alluded to above.) The experimental graphs clearly agree well with the simulations for $\lambda_{in} = \lambda_{el}$, while the values of λ_{in} derived from the experimental data described by Egerton (1986), as also given in Table 3, are clearly inconsistent with our data. This further confirms that the major discrepancy between the theoretical and experimental profile shown in Fig. 5 does not have its origin in a systematic error in the measurement of the specimen thickness.

The fact that the effects of surface contamination are lower than for the first series is also apparent in Fig. 8, which shows graphs of experimental fringe contrast plotted as a function of defocus for a specimen thickness of $0{\cdot}09\lambda_{in}$. There is now less asymmetry with defocus visible in the unfiltered data than for the first specimen. It is also clear that the fringe contrast is increased by 30–50% simply as a result of inserting the virtual objective aperture, suggesting that the main effect of contributions to the images by both the elastic and inelastic scattering of electrons to high angles is to provide a uniform background to the intensity.*

*For the data obtained without an objective aperture we noted a change in the vacuum intensity level between the filtered and unfiltered data of some 10–20%. The main origin of this effect is scattering inside the spectrometer when using an entrance aperture which is larger than 3 mm (as was the case for the data described). Although the effects are smaller when using an objective aperture, uniform backgrounds of 15% for the unfiltered and 10% for the filtered data remained and needed to be subtracted. By comparison with simply scaling the background intensities to the same value, the effect of this is to make calculations of the specimen thickness some 5% greater than without the appropriate background subtraction. The numerical data provided in Table 2 for the second experiments (but not for the first), and as discussed below, were obtained using the correct specimen thickness as obtained after the relevant background subtractions.

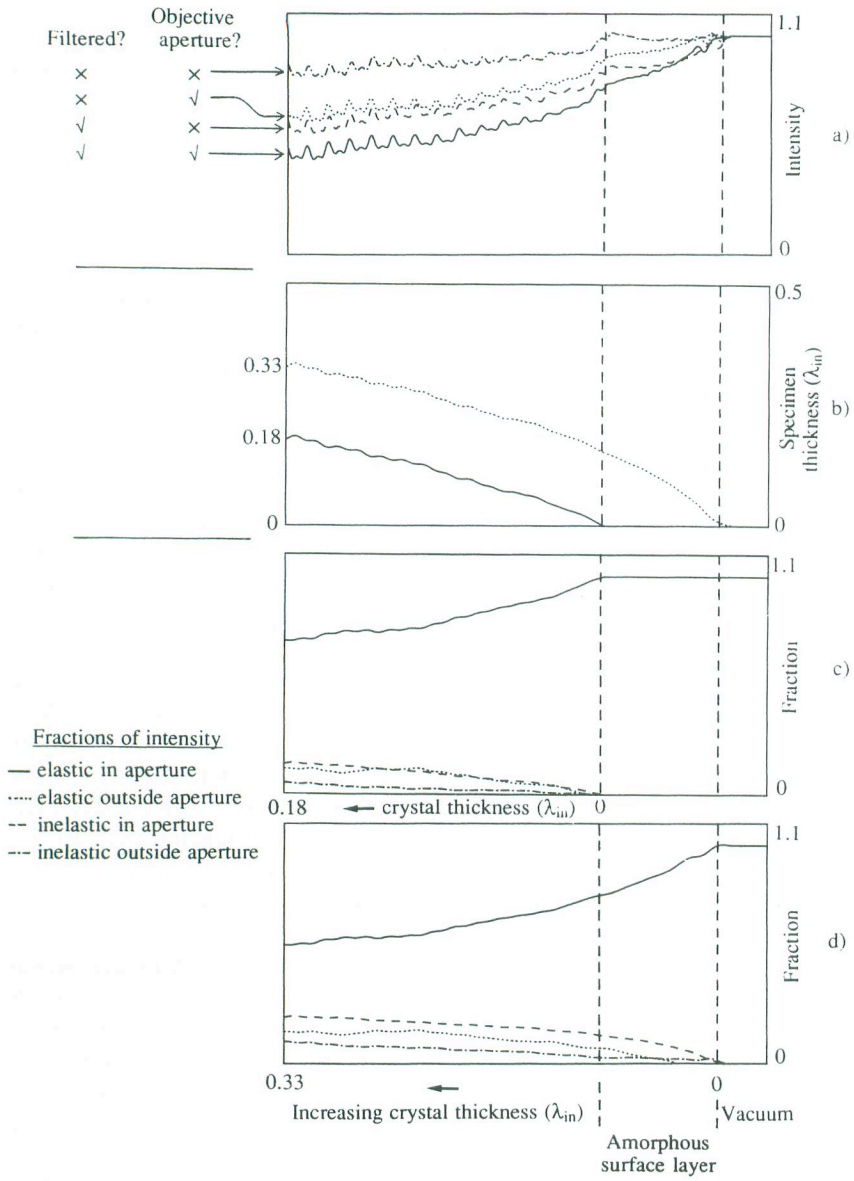

Fig. 6. Analysis of filtered and unfiltered images taken with and without using a 4·5-mrad objective aperture: (a) projections parallel to the layers over a distance of 17 nm (250 pixels), with the vacuum intensities scaled to unity, for images taken four steps overfocus; (b) specimen thickness profile in multiples of λ_{in}, determined both with (——) and without (. . . . .) scaling the intensity at zero *crystal* thickness to unity; (c, d) the fractions of the total intensity in the image which are scattered elastically and inelastically into and outside the objective aperture, with and without scaling the intensity at zero crystal thickness to unity, respectively—the graphs have been calculated from smoothed versions of the profiles shown in (a).

However, a comparison of the effects of filtering for the apertured and unapertured data in Fig. 8 indicates that the fractional increase in contrast for the unapertured data is far larger than for the results using an aperture. This indicates that the higher angle inelastic scattering reduces the contrast more than does the lower angle scattering, and does not simply contribute to a uniform background but to the contrast itself, in a manner such as that described for the image simulations in Fig. 5(b). Consistently with our concern over the lack of agreement of the change in contrast between the experimental and simulated profiles on filtering, as shown in Fig. 5, it appears that the effect of the inelastic scattering on the contrast, even when using an objective aperture when the change is about 30%, is larger than would be predicted on the basis of the inelastic contributions being fully incoherent. Further work in this area is required; here we must concentrate on the more major problem that even when using an aperture the filtered data exhibit considerably lower contrast than would be predicted for the model of the layering used for the simulations in Fig. 5. The remaining experimental parameter that needs to be assessed is the point spread function of the detector in the GIF.

The effect of the response of the detector

For the data described above, the point response of the CCD array of the spectrometer was not taken into account. Figure 9(a) shows an experimentally measured modulation

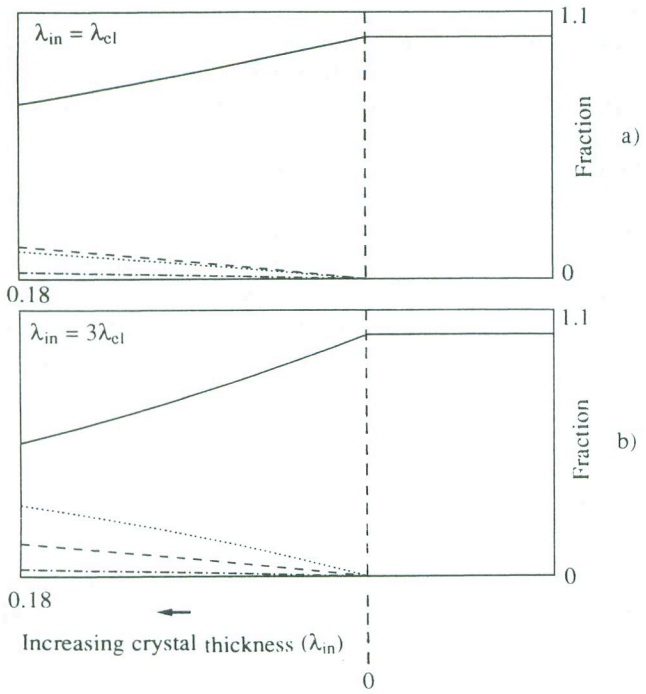

Fig. 7. Simulations of the graphs shown in Fig. 6(c) for a value of λ_{in} of (a) λ_{el} and (b) $3\lambda_{el}$ (see text for details).

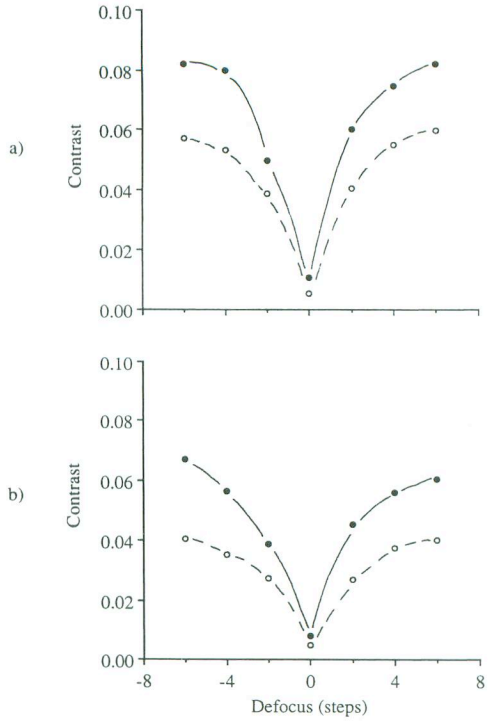

Fig. 8. First fringe contrast plotted for the images obtained (a) with and (b) without an objective aperture, for a specimen thickness of $0{\cdot}09\lambda_{in}$ and for both filtered (——) and unfiltered (- - -) data.

transfer function for the detector: the low-frequency end of the graph was obtained from an image of the edge of a selected-area aperture while the high-frequency end was obtained from the Fourier transform of Poisson noise inherent in uniform illumination; the least noisy parts of the two graphs were merged. The former approach could not be used at high frequencies because the aperture edge did not provide a sharp enough cut off for the electron beam and the latter method could not be used at low frequencies because of noise. It should be recognized that although the modulation transfer function thus obtained could be in error in detail, the effect of any such errors on the deconvolution procedure will be small as the contrast features of interest are always fairly large relative to the pixel size. In order to illustrate the effect of the response of the detector on the data, the graph in Fig. 9(a) was applied to the filtered data of Fig. 6 which had been obtained using an objective aperture. This is illustrated for the four-step overfocus image in Fig. 9(b)—the contrast (and the noise) in both the main and the subsidiary Fresnel fringes is increased by about 15% when the point spread of the detector is deconvoluted in this manner, while the features present are of course unchanged. Figure 9(c) shows the effect of the detector response on the contrast for the filtered data taken using an objective aperture, for a specimen thickness of $0{\cdot}09\lambda_{in}$. It is this final contrast curve with the detector response deconvoluted which must be compared with simulations obtained for different models of the form of the multilayer.

Table 3. Elastic and inelastic mean free paths for Cu at 400 kV, obtained from both the equations and the experimental data presented in Egerton (1986) (see text for details).

	Calculated values			Experimental data converted to 400 kV
	To all angles	Into 4·5-μm aperture	Fraction scattered into aperture	To all angles
Inelastic	68	83	0·82	91–148
Elastic	48	161	0·30	—

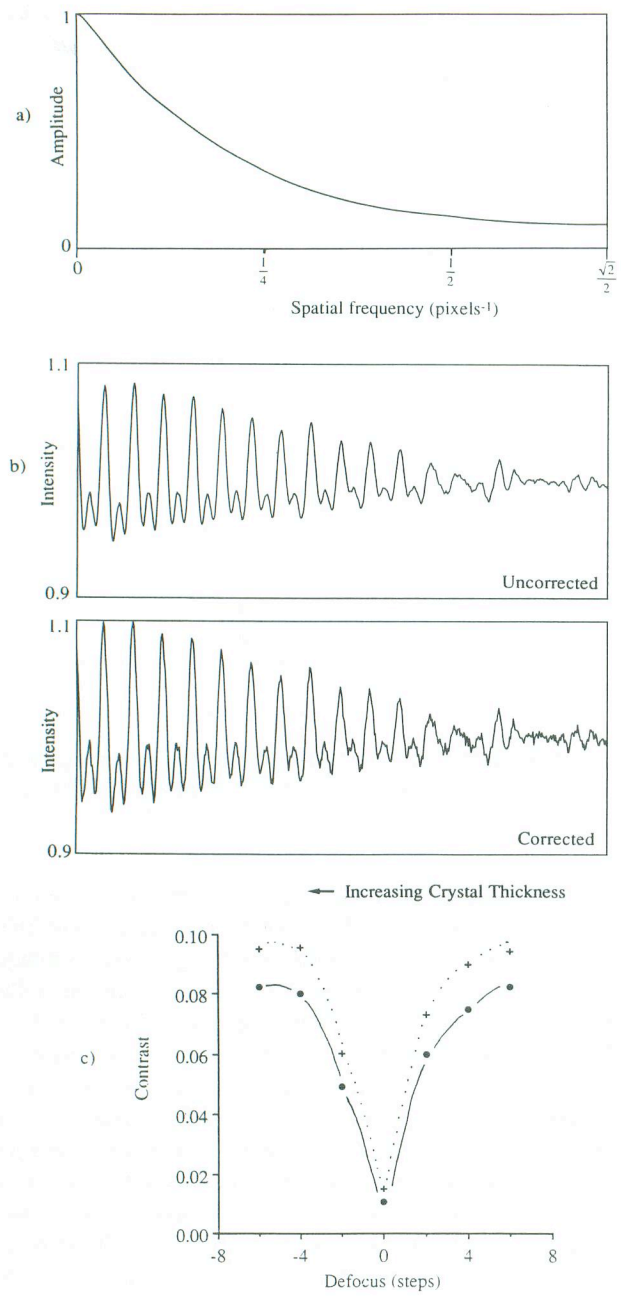

Fig. 9. The effect of the response of the detector on the data: (a) modulation transfer function, determined at the low-frequency end from the image of a sharp edge and at the high-frequency end from the Fourier transform of uniform illumination; (b) illustration of the effect of applying the modulation transfer function shown in (a) on the experimental data, in this case for the four-step overfocus filtered image taken using an objective aperture; (c) graph of fringe contrast plotted as a function of defocus for the filtered data obtained using an objective aperture, both before (——) and after (. . . . .) applying the modulation transfer function shown in (a).

The new values for the retained discrepancy between experiment and theory are given in Table 2 and it can be seen that now, with all of the potential contrast-reduction effects having been dealt with (excluding the effect of the long-range waviness of the layering as deduced from Fig. 4b for the higher thicknesses examined here), the experimental contrast is still a factor of 1·8 lower than that which would be predicted on the basis of a conventional elasticity treatment for the multilayer strains. Thus, taking into account the effect of projection as deduced from Fig. 4(b), the experimental contrast would then be some 30% lower than that expected conventionally. Given the attention paid to the ways the contrast seen is altered experimentally, this apparent error is large.

The effect of anomalous multilayer strains

The forward scattering potential, V_0, is of course sensitive to the local density as well as to the composition of the material. It was expected that using filtered data we would be able to test whether the approximation for the layer strains based on a minimum strain energy criterion was better than assuming that the in-plane spacings were constrained to the bulk value for the copper substrate on which the multilayer was epitaxially grown. The latter assumption would indeed change the magnitude of ΔV in the correct sense, but the magnitude of the change in contrast in simulations would be far less than would be required for a match with the experimental data. It is intriguing that Müller *et al.* (1995) have recently shown that there is a structural rearrangement of the Fe atoms in a thin face-centred Fe layer grown on (001) Cu to a depth of about five atomic layers. The results were obtained using LEED for a surface layer, and it is probable that the constrained Fe layers in an epitaxially grown multilayer would not exhibit the same layer spacings as measured by Müller *et al.* (1995), but it is nonetheless interesting to examine the effect of their data to predict a value for ΔV to use for the assessment of the Fresnel data. In such circumstances, the constrained Cu lattice plane spacings could not be evaluated using conventional elasticity theory and we have arbitrarily retained the Cu spacing values from the minimum strain energy calculation while substituting the average Fe out-of-plane lattice plane spacings obtained by Müller *et al.* (1995). The effect on ΔV is large, the conventional elasticity-based value of 4·1 V being reduced to 2·8 V (see Table 2). Simulations were compared with the filtered experimental data with an objective aperture, now modified for the effect of the response function of the detector (Fig. 9c), and it was found that the simulated contrast was only about 20% greater than that obtained experimentally. When it is remembered that it was inferred from Fig. 4(b) that the contrast data obtained at a thickness of $0{\cdot}09\lambda_{in}$ suffer a reduction of about 30% due to the effects

of projecting the long-range waviness of the layering, the agreement between the experimental data and the simulations for this model, which incorporates anomalously large values for the out-of-plane Fe spacings, is remarkably good. Retained uncertainties in the true crystal thickness, as well as in the precise form of the detector response function, correctly preclude any further atomistic modelling, but it is clear that the out-of-plane lattice spacings for the Fe must be very far from those that would be predicted elastically on the basis of cubic unstrained f.c.c. Fe lattice parameters (as extrapolated from their equilibrium high-temperature values). It is thus noteworthy that preliminary HREM data on the relative values of the in-plane and out-of-plane spacings for this multilayer similarly require that the Fe layers are substantially expanded parallel to the multilayer normal (by about 5%), rather than contracted as would have been expected according to conventional elasticity theory (Lloyd *et al.*, 1995).

6. Conclusions

The more direct results of our investigation are as follows.
1 Inelastically scattered electrons contribute significantly both to the background and to the contrast in Fresnel data, and they do so in ways which, while being qualitatively predictable, are difficult to analyse in a quantitative fashion.
2 Filtered Fresnel data cease to exhibit the asymmetries with defocus, which are the signature of inelastic contributions and are not modelled by normal or anomalous absorption treatments.
3 When filtered Fresnel data are obtained, it is nonetheless necessary both to use fairly small objective apertures and to deconvolute the effects of the detector response function if the data are to be quantified for comparison with models for the projected potential of the structure examined.
4 Simulations of the observed filtered Fresnel contrast require that the out-of-plane lattice spacings in the Fe layers differ significantly both in spacing (by about 5%) and in the sense of the spacing change from that extrapolated for f.c.c. iron from the predictions of conventional elasticity theory.

This latter anomaly is of the same type as has been described previously for thin multilayers of Cu/NiPd (Baxter & Stobbs, 1986). Thus, while it is currently popular to claim that any anomalies in the elastic properties of fine multilayers are small, the results described here indicate that the 'stress-free' state of such layers can be far from that which would be predicted on the basis of bulk lattice parameters.

Arguably a secondary, if surprising, conclusion is that it is very difficult to match absolute magnitudes of the contrast from a given heterogeneity (whatever the type of contrast examined) unambiguously when the specimen examined has amorphous contamination. Since specimens of the type examined here have to be made by ion beam thinning, this suggests that the thicker the specimen that can be examined the better, since the relative effects of the contamination on the scattering should then be reduced. This in turn emphasizes the importance of filtering, but it is noteworthy that it was only by the comparison of unfiltered and filtered data as a function of thickness that we were here able to gain confidence in the values used for the specimen thickness.

The amorphous layer clearly results in the addition of both elastic and inelastic backgrounds to the contrast, as well as changing the effective convergence onto the specimen, though reductions in contrast also result from direct contributions from inelastically scattered electrons. It is significant that the contrast asymmetry with defocus is more pronounced for the experimental data than for the simulations, and the more so when the amorphous surface layer is thick. Since we have reasonable confidence in the thickness values, this suggests strongly that the inelastic contrast contributions are to a degree coherent and thus contribute more strongly than if they did so totally incoherently.

References

Baxter, C.S. & Stobbs, W.M. (1986) High resolution lattice imaging reveals a 'phase-transition' in Cu/NiPd multilayers. *Nature*, **322**, 814–816.

Boothroyd, C.B., Dunin-Borkowski, R.E., Humphreys, C.J. & Stobbs, W.M. (1994) Quantifying the effects of amorphous layers on image contrast using energy filtered transmission electron microscopy. *Beam–Solid Interactions for Materials Synthesis* (ed. by D. E. Luzzi, T. F. Heinz, M. Iwaki and D. C. Jacobson), *Mater. Res. Soc. Proc.* **354**, 495–502.

Boothroyd, C.B. & Stobbs, W.M. (1988) The contribution of inelastically scattered electrons to high resolution images of (Al, Ga)As/GaAs heterostructures. *Ultramicroscopy*, **26**, 361–376.

Boothroyd, C.B. & Stobbs, W.M. (1989) The contribution of inelastically scattered electrons to high resolution [110] images of AlAs/GaAs heterostructures. *Ultramicroscopy*, **31**, 259–274.

Dobson, A.S., Preston, A.R. & Stobbs, W.M. (1991) Can the absorption behaviour of superposed layers be fitted simply? *Inst. Phys. Conf. Ser.* **119**, 449–452.

Egerton, R.F. (1986) *Electron Energy-Loss Spectroscopy in the Electron Microscope*. Plenum Press, New York.

Howie, A. (1963) Inelastic scattering of electrons by crystals I. The theory of small-angle inelastic scattering. *Proc. Roy. Soc.* A271, 268–287.

Lloyd, S.J., Somekh, R.E., Dunin-Borkowski, R.E. & Stobbs, W.M. (1994) Structural characterisation of iron-copper multilayers using transmission electron microscopy. *Fractal Aspects of Materials* (ed. by F. Family, P. Meakin, B. Sapoval and R. Wool), *Mater. Res. Soc. Proc.* **367**, 317–322.

Lloyd, S.J., Somekh, R.E. & Stobbs, W.M. (1995) Structural characterisation of Fe–Cu multilayers of differing Fe thicknesses using transmission electron microscopy. *Structure and Properties of Multilayered Thin Films* (ed. by T. D. Nguyen, B. M. Clemens, B. M. Lairson and K. Sato), *Mater. Res. Soc. Proc.* **382**, 155–160.

Moruzzi, V.L., Marcus, P.M. & Kübler, J. (1989) Magnetovolume instabilities and ferromagnetism vs. antiferromagnetism in bulk fcc iron and manganese. *Phys. Rev.* **B39,** 6957–6961.

Müller, S., Bayer, P., Reischl, C., Heinz, K., Feldmann, B., Zillgen, H. & Wuttig, M. (1995) Structural instability of ferromagnetic fcc Fe films on Cu (100). *Phys. Rev. Lett.* **74,** 765–768.

Ness, J.N., Stobbs, W.M. & Page, T.F. (1986) A TEM Fresnel diffraction-based method for characterizing thin grain-boundary and interfacial films. *Phil. Mag.* **A54,** 679–702.

Rez, D., Rez, P. & Grant, I.P. (1994) Dirac-Fock calculations of X-ray-scattering factors and contributions to the mean inner potential for electron-scattering. *Acta Cryst.* **A50,** 481–497.

Ross, F.M. & Stobbs, W.M. (1991a) Computer modelling for Fresnel contrast analysis. *Phil. Mag.* **A63,** 37–70.

Ross, F.M. & Stobbs, W.M. (1991b) A study of the initial stages of the oxidation of silicon using the Fresnel method. *Phil. Mag.* **A63,** 1–36.

Ross, F.M. & Stobbs, W.M. (1991c) The characterisation of GaAs/(Al,Ga)As heterostructure interface roughness using Fresnel analysis. *Ultramicroscopy,* **36,** 331–354.

Somekh, R.E. & Baxter, C.S. (1986) Sputter deposition of single-crystal metal multilayers. *J. Crystal Growth,* **76,** 119–125.

Stobbs, W.M. & Ross, F.M. (1989) The Fresnel method for the characterisation of interfaces. *NATO ASI Series B Physics,* **203,** 183–202.

Stobbs, W.M. & Saxton, W.O. (1988) Quantitative high-resolution transmission electron-microscopy—the need for energy filtering and the advantages of energy-loss imaging. *J. Microsc.* **151,** 171–184.